Understanding image contrast formation in TiO_2 with force spectroscopy

Ayhan Yurtsever,[1] Delia Fernández-Torre,[2] César González,[3] Pavel Jelínek,[4] Pablo Pou,[2] Yoshiaki Sugimoto,[1] Masayuki Abe,[1] Rubén Pérez,[2,*] and Seizo Morita[1]

[1]*Graduate School of Engineering, Osaka University, 2-1 Yamada-Oka, 565-0871 Suita, Osaka, Japan*

[2]*Departamento de Física Teórica de la Materia Condensada, Universidad Autónoma de Madrid, E-28049 Madrid, Spain*

[3]*Instituto de Ciencia de Materiales de Madrid (ICMM-CSIC), E-28049 Madrid, Spain*

[4]*Institute of Physics, Academy of Sciences, Cukrovarnická 10, 162 00, Prague, Czech Republic*

(Received 18 September 2011; revised manuscript received 14 February 2012; published 13 March 2012)

Site-specific force measurements on a rutile TiO_2(110) surface are combined with first-principles calculations in order to clarify the origin of the force contrast and to characterize the tip structures responsible for the two most common imaging modes. Our force data, collected over a broad range of distances, are only consistent with a tip apex contaminated with clusters of surface material. A flexible model tip terminated with an oxygen explains the protrusion mode. For the hole mode we rule out previously proposed Ti-terminated tips, pointing instead to a chemically inert, OH-terminated apex. These two tips, just differing in the terminal H, provide a natural explanation for the frequent contrast changes found in the experiments. As tip-sample contact is difficult to avoid while imaging oxide surfaces, we expect our tip models to be relevant to interpret scanning probe studies of defects and adsorbates on TiO_2 and other technologically relevant metal oxides.

DOI: 10.1103/PhysRevB.85.125416 PACS number(s): 68.37.Ps, 07.05.Tp, 68.47.Gh

I. INTRODUCTION

Titanium dioxide (TiO_2) is used in a broad range of applications, for example, light harvesting, catalysis, surface coating, gas sensing, and medical implants. An atomic-scale understanding of its surface properties and chemistry is essential to optimize most of these processes.[1–3] The most stable facet of TiO_2, rutile TiO_2(110), has become the model oxide surface for these studies. Its structure is characterized by alternating rows of fivefold coordinated Ti atoms (Ti_{5c}) and bridging oxygens (O_b)—protruding ∼1 Å from the surface plane—that run along the [001] direction [see Fig. 2(a) (inset)]. Scanning tunneling microscopy (STM) images usually show perfect bright rows, identified with Ti_{5c},[4] and bright, localized features in between that have been associated with two defect species [oxygen vacancies and hydroxyl (OH) groups] located on the O_b rows.[5,6] At variance with STM, atomic force microscopy with true atomic resolution [known as noncontact (nc)-AFM[7]] has revealed a number of qualitatively different contrast modes.[8–12] Most images show either a contrast similar to STM with Ti_{5c} rows and defects imaged bright and O_b rows imaged dark (protrusion mode), or its complete reversal (O_b bright and Ti_{5c} rows and defects appearing dark), called hole mode. In a third but rather rare mode called neutral, OH groups and the O_b atoms are imaged bright while O_b vacancies and Ti_{5c} rows appear dark. Other noncommon image contrasts include the "all-inclusive mode" where both O_b and Ti_{5c} are simultaneously resolved as bright features[11] and the "hidden mode" which does not exhibit OH groups.[12]

This contrast variability in nc-AFM represents both an opportunity and a challenge. It reflects the extreme dependence of the tip-sample forces on the structure and composition of the tip apex. But, at the same time, it opens the possibility, through a combination of experiments and theoretical modeling, to characterize the tip and to make a direct identification of defects and adsorbates on technologically relevant oxide surfaces. Calculations with model tips, like an MgO cube,[13] provide a basic understanding of the contrast in the protrusion and hole modes in TiO_2 in terms of electrostatic interactions controlled just by the tip apex polarity, as also proposed for other ionic surfaces.[14] The neutral case has been explained as due to the onset of covalent bonding with a nonpolar model Si tip.[10] However, a deeper, quantitative understanding of the contrast and the link with the tip structure requires us to go beyond just nc-AFM imaging. Combining the AFM topography and the simultaneously recorded average STM currents with atomistic simulations, several models based on O- and Ti-terminated clusters attached to a Si tip and different Si apexes have been proposed to explain the five different combinations of AFM/STM contrasts found in the experiments.[15] Force spectroscopy (FS) experiments, in which tip-sample forces are determined as a function of distance for specific surface sites[16] or over a two-dimensional (2D) area (3D mapping),[17] impose an even stronger constrain on the tip structure and the nature of the interactions. FS has been used to discriminate between the two ionic sublattices on several insulator surfaces,[18–22] to achieve single-atom chemical identification on semiconductors,[23] and to understand the nc-AFM contrast on carbon nanostructures.[24,25]

In this work we combine site-specific force measurements and extensive first-principles calculations on TiO_2(110)-1 × 1, aiming to clarify the origin of the observed nc-AFM contrast and to characterize the tip structures responsible for the protrusion and hole imaging modes. While many tip models could be compatible with forces and contrast on typical imaging distances, our data close to the force minima is only consistent with a tip apex contaminated with clusters of surface material. A flexible model tip terminated with an oxygen explains the data obtained for the protrusion mode. For the hole mode, FS data rule out previously proposed Ti-terminated tips, pointing instead to a chemically inert, OH-terminated TiO_2 apex. These two tips, that just differ in the terminal H, provide a natural explanation for the frequent contrast changes found in the experiments.

The rest of the paper is organized as follows. In Sec. II we describe the experimental and theoretical methodology. Section III provides a discussion of our results for the protrusion and hole imaging modes, including a detailed account on the reproducibility of the experimental force curves and the tip models that are consistent with those results. We summarize our findings and main conclusions in Sec. IV. Finally, in two Appendices we discuss the determination of the van der Waals forces between tip and surface and their theoretical treatment.

II. METHODS

A. Experimental details

The experiments were carried out with a home-built ultrahigh-vacuum nc-AFM[26] operated at a temperature of 80 K with a base pressure better than 5×10^{-11} Torr. The nc-AFM instrument was operated under the frequency modulation detection method.[27] The cantilever deflection was measured using a home-made optical interferometer. The images were acquired under the constant oscillation amplitude mode using commercial silicon cantilevers (provided by Nanosensors). Before use, the tips were cleaned using Ar-ion sputtering to remove the native oxide layer and other contaminants. In order to minimize the long-range electrostatic force during both topographic and spectroscopic measurements, the average contact potential difference was compensated by applying a sample bias in the range 0.5–2.5 V, with the tip being held at ground potential. In addition to the capability of the low temperature system for keeping the thermal drift effect at a minimal level, for the force spectroscopic measurements, atom tracking and feed-forward software[28] were used to precisely position the tip on top of target atoms.

A clean rutile $TiO_2(110)$ crystal (provided by Shinko-sha) used in our experiments was prepared using repeated cycles of Ar^+ ion bombardment (2 keV, 3×10^{-6} Torr) for about 5 min at room temperature (RT) and annealing to approximately $\sim$1000 K for 1 min to restore a flat substrate. During the final annealing of the surface, the pressure was kept below 5×10^{-10} Torr. After 1 h of cooling to room temperature, the sample was transferred into an observation chamber that houses the AFM unit at low temperature. The OH groups on the $TiO_2(110)$ surface were spontaneously created from the dissociation of water molecules (from background residual gas) over the oxygen vacancy sites by transferring an H atom to neighboring O_b sites.[5] By keeping the freshly prepared sample in UHV more than 4 h, all of the O vacancies are occupied by OHs. Thus, in our measurements, only the OH groups are considered as surface impurity defects.

Site specific force spectroscopy measurements were performed by recording the frequency shift (Δf) of the first mechanical resonance frequency (f_0) of the cantilever as a function of the tip-sample distance. In total, five approach-retraction frequency shift vs distance measurements have been conducted, and the total frequency shift is the average of these measurements. The frequency shift (Δf) curves have been shifted at the regulation set points for taking into account topographic corrections.[29] After smoothing over ten data points, the averaged Δf curves are converted to total force by using the inversion formula derived by Sader *et al.*[30] The short-range forces were calculated by subtracting the long-range forces from the total forces. The long-range background forces were obtained by fitting the total forces in the tip-sample distance range from 6 to 25 Å to an analytic function given as $A_H R/6(z - z_0)^2$. In Appendix A we show an example of this procedure to extract the short-range forces from the experimental Δf curves.

B. Theoretical modeling

All calculations were done with VASP 4.6,[31] using the projector-augmented-wave method, a plane-wave cutoff of 400 eV, and the Perdew-Burke-Ernzernhof (PBE)[32] functional. We also re-calculated the forces for some of the models using LDA, obtaining the same general trend but overall more attractive interactions.

To represent the $TiO_2(110)$ surface pure and with a hydroxyl defect we constructed supercells of two different sizes, 4×3 and 4×2 (11.9×19.8 Å and 11.9×13.2 Å), which we used depending on the lateral size of the tip model under study. The sampling in k space was done using the Γ point and larger 2×2 Monkhorst-Pack meshes. The slab was two trilayers thick, and the lowermost trilayer was kept fixed to the bulk positions. Although a thicker slab is needed for converging many surface properties of $TiO_2(110)$,[1] the geometry of the uppermost trilayer is well described within the present model, and we thus expect it to produce converged values for the tip-surface interaction forces. For each tip model under study, the lattice parameter perpendicular to the surface was different depending on both the tip size and the largest tip-surface distance, but we made sure that the vacuum left was at least 7 Å.

An important ingredient in our modeling is that we approach the tip to the surface in a quasistatic way, in small steps of 0.25 Å, and for each step we relax the atoms at the bottom of the tip and at the top of the surface until the forces are smaller than 0.04 eV/Å. As we will demonstrate in the next section, the relaxations of the tip are crucial to evaluate the forces at short tip-sample distances.

As an exchange of material between tip and surface is likely to happen in the experiments, we have built our tip models following two different directions (see Fig. 1): (1) silicon-based tips,[33] with their apices contaminated with surface (Ti,O) or H atoms, as proposed in previous works;[11] and (2) small TiO_2 clusters, based on a $(TiO_2)_5$ isomer proposed by Lundqvist *et al.*[34] (in the reference, the model in Fig. 1 C). We rotated the isomer to expose different terminations characteristic of TiO_2 cluster structures: a doubly or a singly coordinated O atom [Figs. 1(c) and 1(d)], and a Ti atom [Fig. 1(h)]. Besides, we also considered the possibility of H contamination for the two O-terminated models [Figs. 1(k) and 1(l)].

III. RESULTS AND DISCUSSION

A. Protrusion mode forces

A typical nc-AFM image in the protrusion mode obtained during our set of experiments, with the sites over which we recorded the FS curves marked with crosses, is displayed in Fig. 2(a). The dissipation signal (not shown) was recorded

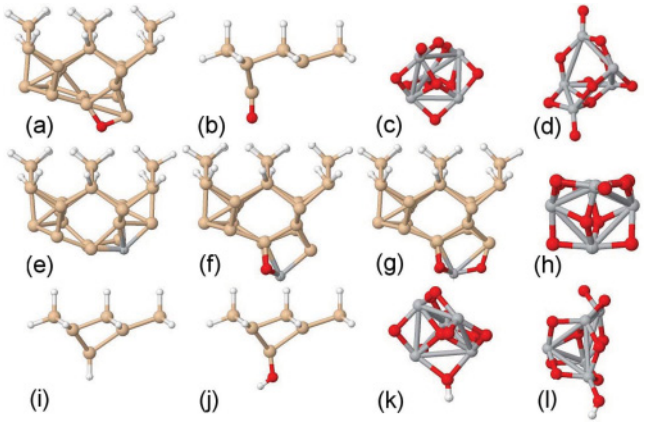

FIG. 1. (Color online) Most relevant tip models tested in this work. (a)–(d) Oxygen-terminated, (e)–(h) Titanium-terminated, and (i)–(l) Hydrogen-terminated. The color code for the ball-and-stick structures is the following: white corresponds to H, red to O, grey to Ti, and cream to Si. The Si-based tips have their apex contaminated with O [(a), (b)], Ti [(e)], Ti and O [(f), (g)], H [(i)], and an OH group [(f)]. Tips (c), (d), (h), (k) and (l) correspond to a $(TiO_2)_5$ isomer[34] rotated to expose different terminations [(c), (d), (h)] and including possible H contamination [(k), (l)].

simultaneously with the forces, and it was site independent and negligible for all distances. Surprisingly, the experimental short-range forces turn out to be attractive for the three sites, with large maximum values over Ti_{5c} and O_b (about 1.6 and 1.2 nN, respectively). Moreover, these maximum forces are reached after a decay that is too steep to be caused by pure electrostatic interactions, as it has been assumed in previous nc-AFM works. Interestingly, the curves over Ti_{5c} and O_b for $d < 2$ Å are remarkably parallel to each other.

The reproducibility of the protrusion mode forces was very good in all our experiments performed with different tips and cantilevers. An example of forces measured on the same area displayed in Fig. 2(a) and with identical tip conditions (including tip termination) but over different O_b and Ti_{5c} sites is shown in Fig. 3(a). Force curves obtained with another tip on a different surface area are displayed in Fig. 3(b). In both cases, the results are very similar to those in Fig. 2(a). Results of this kind have been repeatedly observed during independent experimental runs, so we can conclude that protrusion mode forces are indeed reproducible and do not show a significant tip dependence.

To explain these results, we have calculated force curves on the relevant surface sites for several tip models. Based either on the contrast they produce at typical imaging distances[11] or the values at the force minima, our calculations rule out the contaminated Si tips. Among the TiO_2 tip models, the structure which best reproduces the measured forces is a cluster rotated to expose a singly coordinated oxygen atom at the apex [see model in Fig. 1(d)]. Figure 2(b) shows that the agreement between the measured and calculated forces is very good apart from the repulsive stretch at the O_b site for distances between 1.75 and 3.5 Å found in the simulations. Furthermore, this tip does not present hysteresis in an approach-retraction cycle (not shown), in line with the experiments.

One of the most striking features in Fig. 2(b), for a nominally "negative tip," like the one we are considering, is the large attractive force found when approaching the O_b atoms. The way in which the tip relaxes over this site is the key to explain the measured forces. At long tip-sample distances, the tip undergoes little relaxation, but, upon approaching, the O atom at the tip apex and the surface O_b start to repel each other, and the tip oxygen starts moving away. At short distances, the relaxation is already completed [see models of Fig. 2(b)], and a Ti atom is now at the tip apex. This Ti atom interacts and forms a bond with the surface O_b (confirmed by a charge pileup between these atoms), explaining the large force minimum and the fast decay of the experimental forces. This interaction

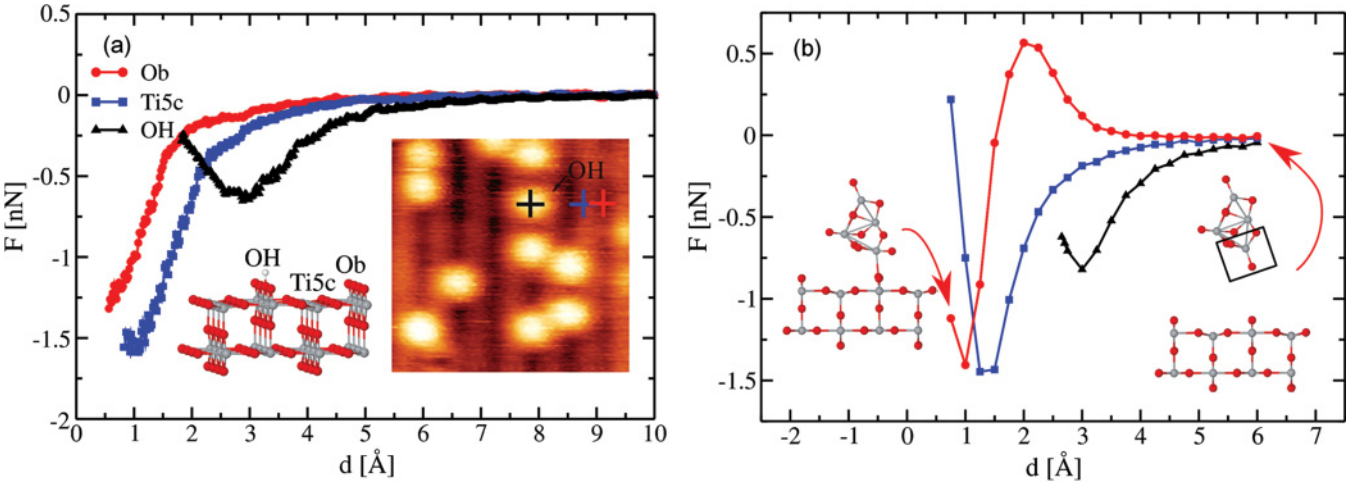

FIG. 2. (Color online) (a) Experimental short-range forces on TiO_2(110) for the protrusion mode image contrast shown in the inset. The studied sites are: bridging oxygens (O_b, red dots), fivefold-coordinated Ti atoms (Ti_{5c}, blue squares), and hydroxyl defects (OH, black triangles). Another inset illustrates the surface structure: O (Ti) atoms are displayed as red (gray) balls, H atoms as white. (b) Calculated short-range forces over the same sites considered in (a). Insets: ball-and-stick models of the tip and surface structure over the O_b site at $d = 0.75$ Å and $d = 6$ Å (d is measured with respect to the O_b atoms). The d axis of the experimental force curves has been shifted to adjust the position of the attractive force maximum of the OH site to the theoretical one (d $\sim$ 3 Å).

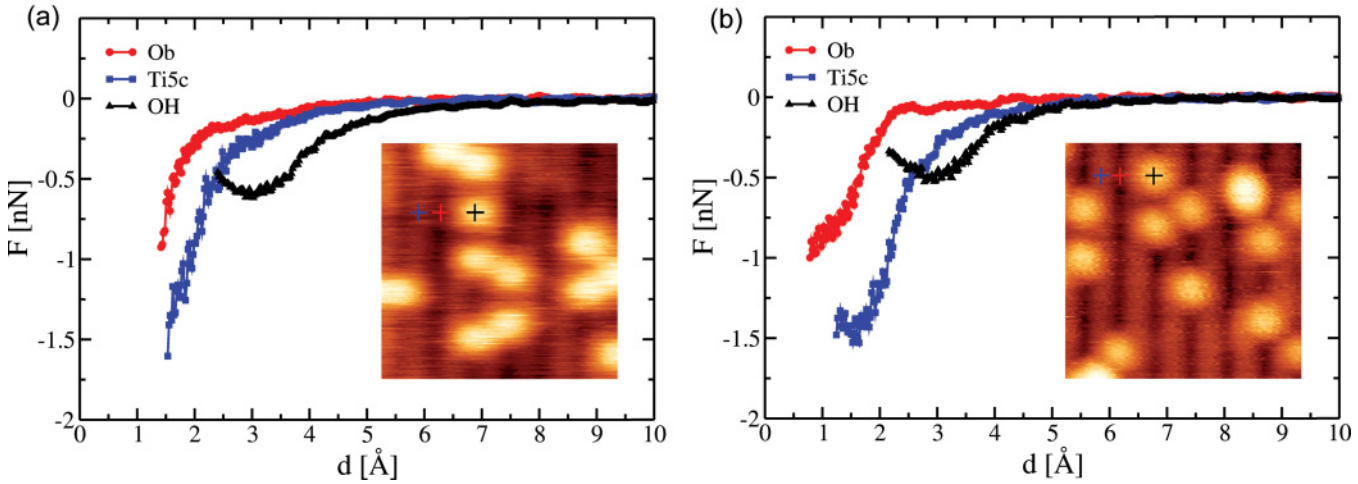

FIG. 3. (Color online) Reproducibility of the force curves obtained during the experiments with tip terminations producing protrusion mode contrast images. The color code and notation are the same as in Fig. 2. Each d axis has been shifted to place the OH minimum at $d \sim 3$ Å. (a) Forces measured on the same area displayed in Fig. 2(a) and with identical tip conditions (including tip termination) but over different O_b and Ti_{5c} sites. (b) Force curves obtained with another tip on a different surface area. These results prove that protrusion mode forces are reproducible and do not show a significant tip dependence.

mechanism is further confirmed by the similarity in both the experimental and calculated force minima for the Ti_{5c} and O_b sites. At variance, around the minimum at the OH site, we have a weaker interaction that is dominated by the hydrogen bond between the surface hydroxyl and the oxygen in the tip apex and includes also electrostatic contributions. It could be assumed that a large van der Waals (vdW) background would be necessary to provide a net attractive interaction for a "negative" tip approaching the O_b sites. The relaxation of the TiO_2 tip to expose a Ti atom at the apex close to the force minimum shows that this is not the case. In fact, the vdW forces measured in the experiment are significantly smaller than the short-range forces (see Appendix A), giving further support to our proposed tip model. The flexibility of the tip controls the energetics of such relaxation at the apex. Due to the computational cost, we have modeled it with a small $(TiO_2)_5$ cluster where only the last five atoms were allowed to relax [see Fig. 2(b)]. Thus we assign the repulsive stretch in the O_b force curve to our very limited description of the elastic properties of the tip as a whole. This characteristic relaxation is not private to the singly coordinated oxygen atom at the apex. We have found the same structural changes and very similar force curves for the same cluster rotated to expose a doubly coordinated oxygen [see Fig. 1(c)], but the repulsive force overshoot was larger. Given our limited tip size, we cannot rule out completely any of these two energetically favorable terminations. More importantly, the common behavior confirms that oxide-based tip models are really necessary to explain our FS data.

B. Hole mode forces

We now move to the analysis of the hole mode in $TiO_2(110)$. Figure 4(a) shows the short-range forces measured above the three lattice sites (O_b, Ti, and OH) marked with crosses in the

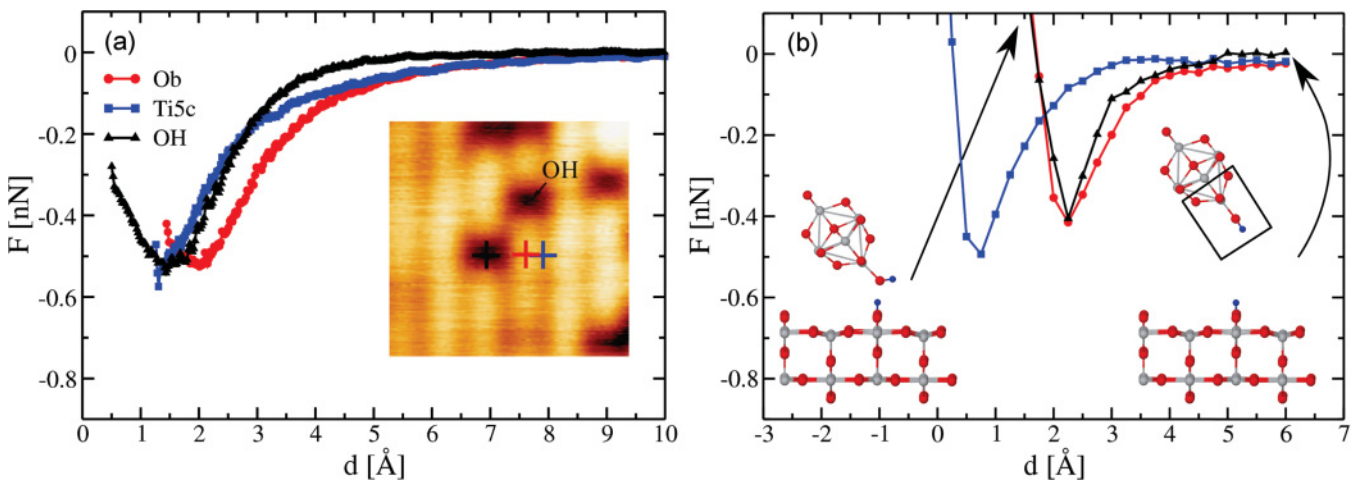

FIG. 4. (Color online) (a) Experimental and (b) calculated short-range forces for the hole imaging mode (definitions as in Fig. 2). The tip and surface relaxed structures over the OH site in (b) correspond to $d = 1.5$ Å and $d = 6$ Å.

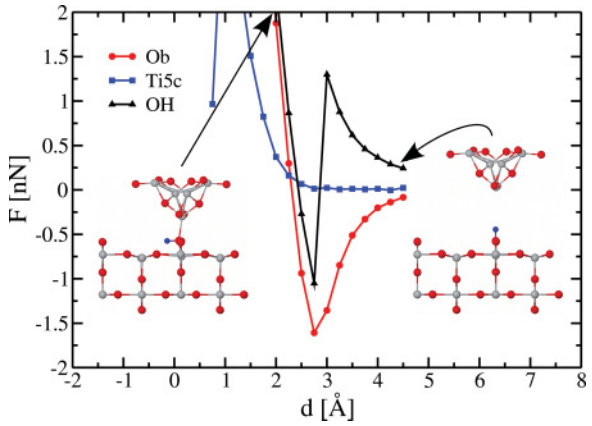

FIG. 5. (Color online) Calculated force vs distance curves for a TiO_2 based, Ti-terminated tip model. The color code and the structure representation of the insets are analogous to those in Fig. 2. The arrows indicate the force points which correspond to each structure in the inset.

inset image. Once again the dissipation signal is negligible for all sites. At large to medium tip-sample distances, the smallest forces are measured over the OH site, and the strongest over the O_b, which consequently appear, respectively, as dark spots and bright stripes in the nc-AFM image. At shorter distances, all the force curves reach almost the same attractive force maximum of about 0.5 nN. It is interesting to notice the similarity between the FS curves under discussion and the experimental forces in the protrusion mode over the OH site discussed previously.

We started our search over tip model candidates based on Si tips and TiO_2 clusters terminated with Ti similar to those proposed previously to explain simultaneously recorded nc-AFM and STM images.[15] All of them consistently produced force minima several times larger than those in the experiment. These minima were always accompanied by large structural relaxations in which the Ti atom protrudes to bind covalently to the nearest surface oxygen atoms available. To illustrate this point with an example, we show in Fig. 5 the calculated forces over the three surface sites when the tip is modeled with a Ti-terminated cluster [see Fig. 1(h)]. The scale for the forces in this figure is much larger than that used in Fig. 4, and we observe large repulsion stretches over OH and Ti_{5c}. Although at long distances the ordering of the curves is consistent with a hole mode contrast, the forces and the force differences among sites are qualitatively different than those observed in the experiments. The same qualitative disagreement between theory and experiment was also found for different Ti-terminated tip candidates such as those illustrated in Fig. 1. As neither the magnitude of the forces nor the force differences between sites were comparable to those in the experiment, we ruled out the titanium terminated tip models.

We next considered tips terminated with an OH group, assuming that the hydrogen can be easily picked up from the surface or produced as a result of collisions with water molecules from the background residual gas. These tips produce minima of the force much closer to experimental values. The model with the best overall agreement, a singly coordinated O termination with an H atom attached, is displayed in Fig. 4(b). The calculated force curves [Fig. 4(b)] over the different sites are parallel to each other, as observed in the experiment. Over the O_b and OH sites, this is probably caused by the formation of similar hydrogen bonds, which control the tip-surface interaction. The two insets in Fig. 4(b) show the tip and sample structure when imaging the OH site for far and close distances. Notice the bending movement of the tip H induced by the tip-sample interactions. This same effect has been observed previously in a Si-based, OH-terminated tip model used to explain the neutral nc-AFM contrast in TiO_2.[11] For the Ti site, the bending of the H atom allows a stronger O-Ti interaction at close distances, but the OH distance is small and the electrostatic screening quite effective, reducing the maximum force.

We have found very similar results for a tip formed attaching an H atom to a doubly coordinated O termination. These

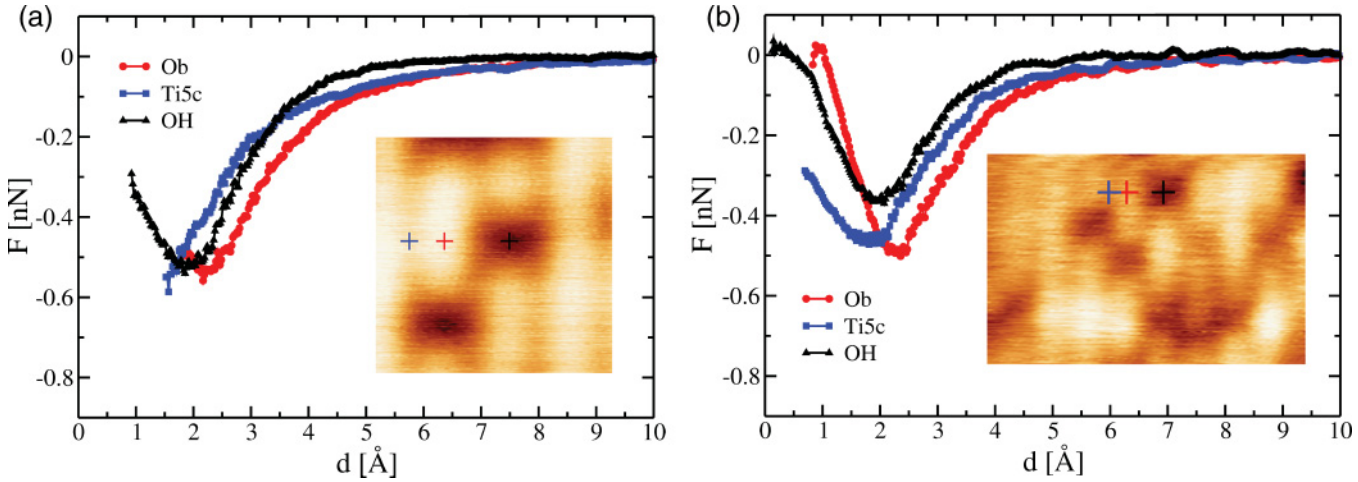

FIG. 6. (Color online) Representative sample of experimental force curves obtained for images showing hole mode contrast. (a) Forces measured on the same area displayed in Fig. 4(a) but with a different tip. (b) Forces recorded on a different experimental run performed with a different cantilever and tip. This latter case illustrates that force curves in the hole, although qualitatively similar in all cases, show a variability in the strength and relatively position of the force maxima. The color code and notation are the same as in Fig. 2. Each d axis has been shifted to put the O_b minimum at $d \sim 2.25$ Å.

calculations show that, although the force strength is consistent with the formation of an H bond, electrostatic interactions which are very dependent on the particular orientation of the tip (e.g., if the two Ti atoms above the OH are aligned with the O_b rows) can increase the force minimum by up to 80% when approaching the O_b sites compared to the OH defects (see next section). We think that this combination of H bonding and electrostatic interactions can explain the contrast variability found for "positive" tips both in our results and in previous experiments.[10]

1. Variability in the experimental forces

While in the protrusion mode all measured force sets were almost identical, in the hole mode there is a small variation in the position and absolute value of the force minima of the curves on the three probed sites (OH, O_b, and Ti_{5c}) for certain measurements. As we already anticipated in the previous section and discussed in more detail below, this tip dependence can be understood in terms of additional electrostatic interactions, that can be either repulsive or attractive depending on the tip structure, that sum up to the main contribution, the formation of the H bond, and modulate the force strength on the different sites.

The first set of results is shown in Fig. 6(a), and corresponds to a tip different from the one used for the measurements in Fig. 4(a), but sampling the same surface area. The similarity between these data and those in Fig. 4(a) is evident. The second set belongs to a different experimental run performed with another cantilever and another tip. In this case, the recorded force curves, although qualitatively similar, show some differences in the strength of the forces. In particular, the force minimum over the OH site occurs at about 0.35 nN, while for the other sets its value was close to 0.5 nN. We have observed similar changes in the relative value of the force minima measured on the three probed sites in several independent experimental runs. The largest difference corresponds to a set where the O_b force minimum was close to 0.8 nN, instead of the 0.5–0.6 nN found in most of the measurements.

2. Calculations with different OH-terminated tips

The forces calculated with different OH-terminated tips clearly show the basic features of the force spectroscopy measurements. Moreover, they also reproduce the variability found in the experiments. Figure 7 illustrates this point with the forces calculated for three additional tip models. The first one is the same tip discussed in Fig. 4(b) but oriented parallel to the surface normal [see inset in Fig. 7(a)]. The corresponding forces (filled symbols) are almost identical to the ones presented for the OH and O_b sites in Fig. 4, while they vary a little for the Ti_{5c} site, where the minimum of the force is about 0.2 nN deeper—the force curve for the tip discussed in Fig. 4 over the Ti_{5c} site (empty symbols) is included for comparison.

The two other cases discussed here correspond to a different OH-terminated TiO_2 cluster with two different orientations with respect to the substrate. Three of the force curves in Fig. 7(b) (filled symbols) are calculated with a cluster where the triangle spanned by the O atom in the OH group and the two neighboring Ti atoms above is parallel to the O_b rows. The fourth curve (empty symbols) corresponds to the calculation over the O_b site with the same cluster rotated 90° around the surface normal, so the Ti-O-Ti triangle is perpendicular to the O_b rows. Comparing the first case with the results presented in Fig. 4, we observe once more some relative changes in the force minima, but now the O_b site is the most affected, with a force minima 80% deeper. The rotated model, however,

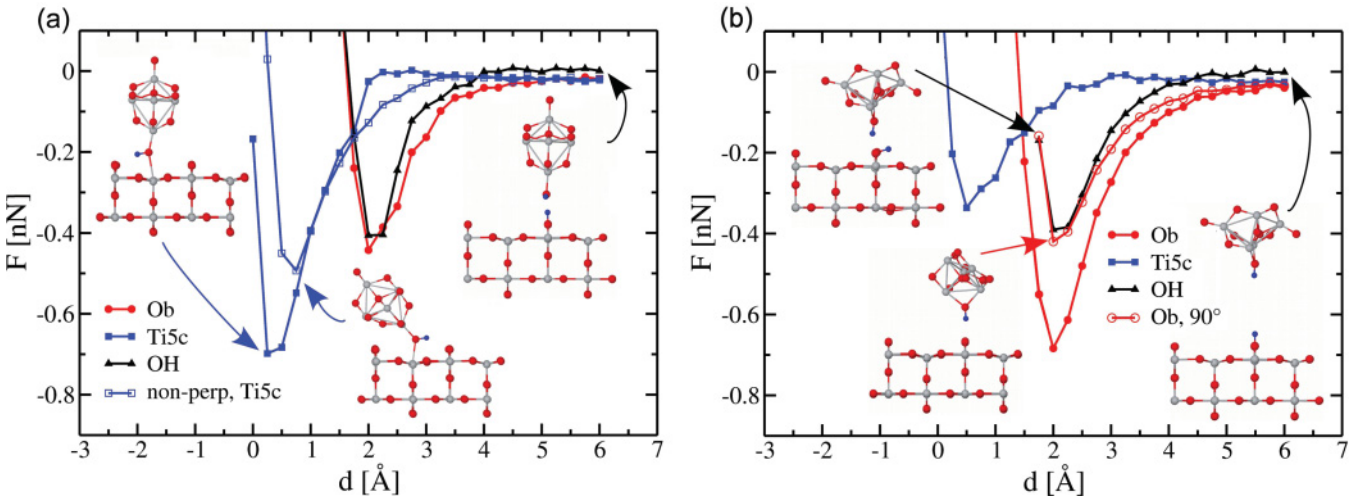

FIG. 7. (Color online) Calculated force vs distance curves for three TiO_2 based, OH-terminated tip models. The color code and the structure representation of the insets are analogous to those in Fig. 2. The arrows join the structures of the insets with their corresponding force values. (a) Filled symbols: Forces over the three surface sites for the tip oriented perpendicularly to the surface. Empty symbols: Force over the Ti_{5c} site for the rotated cluster considered in Fig. 4. (b) Filled symbols: forces over the three surface sites for the tip model shown in the insets at the top left and the bottom right part of the panel, where the triangle spanned by the O atom in the OH group and the two neighboring Ti atoms above is parallel to the O_b rows. Empty symbols: Force curve calculated over the O_b site with the same cluster rotated 90° around the surface normal, so the Ti-O-Ti triangle is perpendicular to the O_b rows (structure shown in the inset in the bottom left part of the figure).

brings the force minima over the O_b site back to the value of ~ -0.4 nN found in Figs. 7(a) and 4.

As the structures in the insets of Fig. 7 show, the main mechanism responsible for the tip-sample interaction is still the formation of the hydrogen bond at short distances discussed before, but now we can assign the small modulation in the forces found both in the experiments and the calculations to additional electrostatic interactions that are controlled by the different detailed arrangement of the atoms surrounding the OH at the tip apex. The two tip models presented in Fig. 7(b), differing just in a rotation around the surface normal, clearly illustrate this point. The forces indicated with filled symbols correspond to the cluster where the two Ti atoms near the apex are aligned along the O_b row. This configuration of the Ti atoms provides some extra electrostatic attraction that makes the O_b force minimum deeper than in the rest of the cases. Upon a 90° rotation, the Ti atoms are moved further away from the surface O_b sites, and thus the minimum over O_b goes back to its usual observed value (about -0.4 nN).

Electrostatic interactions are also responsible for the larger attractive force over the Ti_{5c} found in Fig. 7(a) for the cluster oriented normal to the surface. In the case of the rotated cluster discussed in Fig. 4, one of the oxygens on the side of the cluster comes very close to one of the O_b rows when the tip approaches the Ti_{5c} site [see inset in Fig. 7(a)]. The resulting repulsive interaction (not present for the perpendicularly oriented cluster) reduces the main attractive interaction between the surface Ti atom and the OH group at the tip apex. These additional electrostatic interactions are also present in the protrusion mode case, but as the main apex-substrate interaction is significantly stronger than in the hole mode case, they have a very limited impact in the total observed interaction.

Notice that not only the strength but also the position of the force maximum is modulated by the detailed tip structure. It is difficult to determine precisely the experimental variation in the relative position of the force curves due to the fact that, in many cases [as in Figs. 4 and 6(a)], the force maximum on the Ti atoms cannot be clearly identified. The experiments in Fig. 6(b), where this position is clearly resolved, show a separation of 0.7 Å, smaller than the ~1.5 Å found in the theoretical results in Fig. 4. The main contribution to the theoretical value comes from a purely geometrical effect as the Ti_{5c} atoms are about 1.1 Å lower than the bridging oxygen atoms. Furthermore, in order to have some significant interaction with the Ti_{5c} atom, our sharp tip apex needs to get closer here than over other sites. Here is where

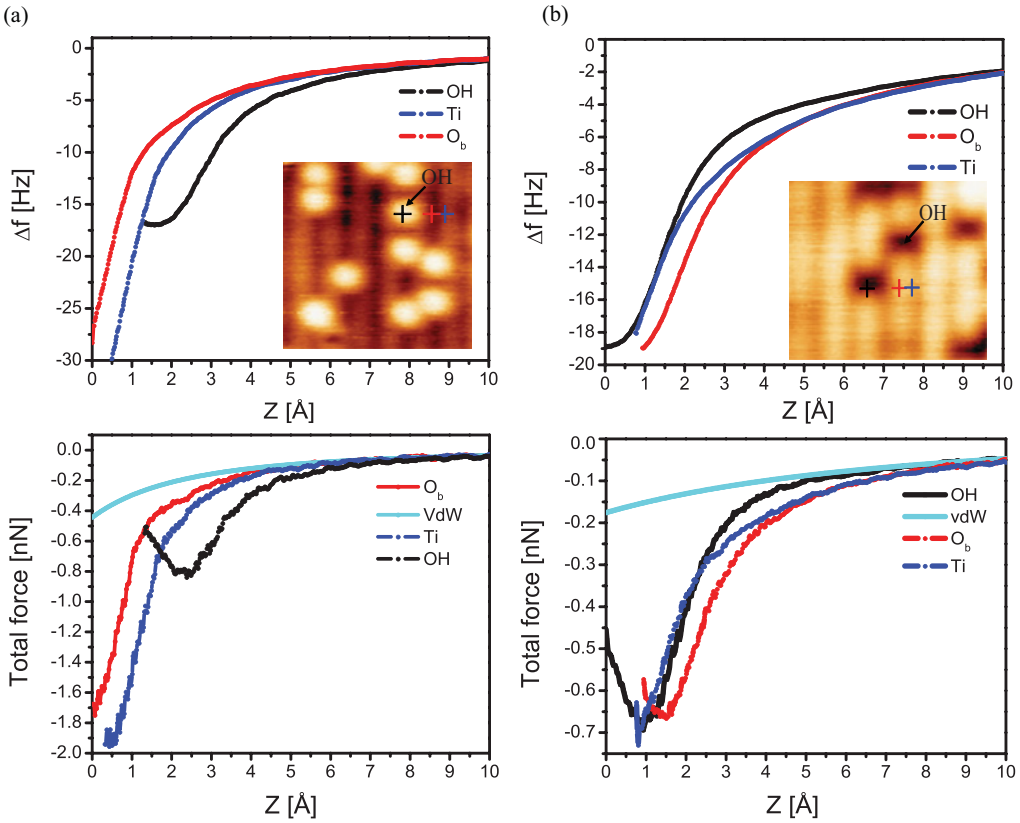

FIG. 8. (Color online) The averaged $\Delta f(Z)$ curves and corresponding total interaction forces measured over the surface atomic and defect sites indicated in the inset topography image (a) for protrusion mode and (b) for hole mode. The short-range force curves shown in Figs. 2(a) and 4(a) (Sec. III) were calculated from the frequency shift curves displayed in (a) and (b). The light blue lines were fitted to the long-range background forces. The acquisition parameters were: (a) $Q = 173\,000$, $K = 30.4$ N/m, $f_0 = 137.762$ kHz, $V_{cpd} = 1.0$ V, and $A = 12.7$ nm. (b) $Q = 224\,000$, $K = 33.8$ N/m, $f_0 = 142.691$ kHz, $V_{cpd} = 2.2$ V, and $A = 10.4$ nm. Image parameters: (a) 4.6×4.6 nm^2 and $\Delta f = -7.4$ Hz; (b) 4.2×4.2 nm^2 and $\Delta f = -7.4$ Hz.

the detailed atomic arrangement around the protruding OH group plays a crucial role. Figure 7(a) illustrates again this point: the tip oriented perpendicular to the surface has a larger force maximum at a closer distance than the "blunter" rotated tip, where the additional electrostatic repulsion among neighboring oxygen atoms reduces the total interaction and moves the force maxima away from the surface. This result implies that, larger tip models, that are beyond the capabilities of *ab initio* methods, would be necessary in order to have a perfect match between theory and experiment for each particular tip.

IV. CONCLUSIONS

The strong requirements imposed by the FS data on the tip models paves the way to clarify the complex FM-AFM imaging scenario with a simple and elegant solution. Our calculations show that the common protrusion and hole mode can only be consistently explained with TiO_2 clusters at the tip apex. Only if particular care is taken to avoid contamination with surface material, we can have Si tips with just an O or OH atom at the apex that provide the rare neutral and "all-inclusive" modes. Our experimental difficulties to perform FS with neutral tips due to tip changes during the force curve acquisition confirm the strong tendency to contamination. Furthermore, these tip models explain the frequent contrast changes while imaging the surface: only the addition/removal of a single H atom is required to change the imaging mode. Our calculations do show these proton transfer events at distances closer than the force minima. The oxygen-terminated tip picks up the proton from the surface OH for $d < 2.65$ Å. Similarly, the OH-terminated tip donates its proton to the TiO_2 surface for $d < 1.5$ Å. While in the protrusion mode all measured force sets were almost identical, in the hole mode there is a small variation in the position and absolute value of the force minima of the curves on the three probed sites (OH, O_b and Ti_{5c}) for certain measurements. Our calculations show conclusively that this tip dependence (also found in previous experiments[10]) can be understood in terms of additional electrostatic interactions, that can be either repulsive or attractive depending on the tip structure, that sum up to the main contribution, the formation of the H bond, and modulate the force strength on the different sites. We believe that similar interaction mechanisms and tip models can be applied to model and understand nc-AFM imaging on other oxide surfaces. In particular, an FS study of the NiO surface has reported attractive forces with minima at 1.6 and at 2.3 nN,[18] very close to the values obtained here for the protrusion mode.

ACKNOWLEDGMENTS

We thank the MEXT (19053006, 22221006, 21246010, 21656013, 20760024, and 22760028), JST, Handai FRC (Japan), and the spanish MICINN (MAT2008-1497, CSD2007-41, MAT2008-02929, MAT2008-02939-E, MAT2008-02953-E, PLE2009-0061, CSD2010-00024) for financial support. P.J. thanks ME10076. Y.S., C.G., and P.P. thank, respectively, Funding Program for Next Generation World-Leading Researchers, a CSIC JAE-Doc contract, and the Ramon y Cajal Program (MICINN). Computer time provided by the RES at the Magerit supercomputer (CesViMa, Madrid, Spain).

APPENDIX A: LONG-RANGE VAN DER WAALS FORCES

The experimental long-range van der Waals forces between tip and surface can be determined using the method described in Sec. II A. Here we show how these forces were extracted for the data sets of Figs. 2(a) and 4(a) that we used for the discussion of the protrusion and hole imaging modes (Sec. III). In Figs. 8(a) and 8(b) we represent the corresponding frequency shift curves registered over the different surface sites (O_b, Ti_{5f}, and OH). By using the Sader inversion algorithm,[30] we obtained the total force data shown in the lower panel of Fig. 8. By fitting the long-distance part of these force curves to the analytic function $A_H R/6(z - z_0)^2$, we obtained the long-range van der Waals forces between tip and sample for both experiments (light blue curves). These van der Waals forces are responsible for the slow decay of the total forces, and also are a non-negligible contribution at short distances, for example, in the hole mode (Fig. 8(b), lower panel), they account for more than 20% of the total.

APPENDIX B: CALCULATED SHORT-RANGE FORCES: CHEMICAL AND VAN DER WAALS CONTRIBUTIONS

We have tested the effect of including van der Waals (vdW) interactions between the slab and the tip model in our theoretical description by adding semiempirical corrections to the PBE functional.[35] The corrections were applied to structures relaxed with PBE. We have used the standard Grimme's parametrization (DFT-D2)[35] which was developed to represent neutral atomic species. As in TiO_2 the atoms have a marked ionic character, some of the calculations were repeated using a set of parameters specially adapted to describe ionocovalent TiO_2.[36] This approach has been applied successfully to predict the stability of the different phases of titania. The vdW energies and forces obtained with this parametrization turned out to be larger than those based on DFT-D2. These results can be explained by the much larger

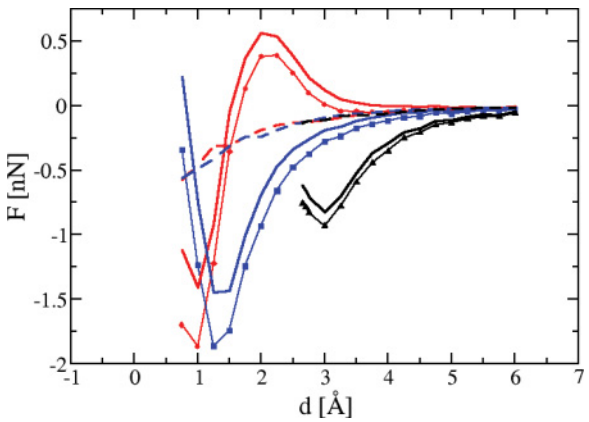

FIG. 9. (Color online) Calculated short-range forces for the tip model in Fig. 1(d). The different curves refer to different surface sites: red is for O_b, blue for Ti_{5c}, and black for OH. The lines with filled symbols correspond to total forces, those without symbols to PBE forces, and the dashed lines to van der Waals forces.

polarizability of the O ions in the ionic model, and the fact that the O-O interatomic distances associated with tip and surface atoms are shorter than their Ti-Ti counterparts.

The methodology used here naturally separates the van der Waals from the rest of chemical contributions to the force. We display these two components and also the total forces in Fig. 9. for the model tip of Fig. 1(d) and the DFT-D2 approach. This tip has been used in Sec. III A to explain the experimental forces of the protrusion imaging mode. The van der Waals forces are the same for the three sites except at short tip-sample distances, see $d = 1$–1.5 Å and $d = 2$–2.5 Å in Fig. 9. In these two regions the dispersive forces over O_b and Ti_{5c} are slightly different because the tip structures also differ [see insets of Fig. 2(b)] due to the action of strong chemical forces. Therefore, in general terms, the short-range van der Waals force does not affect the contrast between sites. However, it affects the magnitude of the total force, especially at short distances or when chemical forces are relatively small. The same trends described here have also been reported in previous theoretical works.[25]

The short-range van der Waals force calculated here (Fig. 9) and the macroscopic van der Waals component obtained from a fit of the experimental forces in Fig. 8 are very similar ($\sim$0.5 nN) at the shortest tip-sample distances. This seems an indication of an overestimation of the dispersive forces by DFT-D2 in TiO_2, and the same applies to the ionic parametrization mentioned at the beginning of this section since it produces even larger values. Due to this, we decided not to include the empirical van der Waals terms into our final theoretical analysis.

*Corresponding author: ruben.perez@uam.es

[1] U. Diebold, Surf. Sci. Rep. **48**, 53 (2003).

[2] C. L. Pang, R. Lindsay, and G. Thornton, Chem. Soc. Rev. **37**, 2328 (2008).

[3] B. Hammer, S. Wendt, and F. Besenbacher, Top. Catal. **53**, 423 (2010).

[4] U. Diebold, J. F. Anderson, K.-O. Ng, and D. Vanderbilt, Phys. Rev. Lett. **77**, 1322 (1996).

[5] S. Wendt, R. Schaub, J. Matthiesen, E. K. Vestergaard, E. Wahlstrom, M. Rasmussen, P. Thostrup, L. Molina, E. Lagsgaard, I. Stensgaard, B. Hammer, and F. Besenbacher, Surf. Sci. **598**, 226 (2005).

[6] O. Bikondoa, C. L. Pang, R. Ithnin, C. A. Muryn, H. Onishi, and G. Thornton, Nat. Mater. **5**, 189 (2006).

[7] S. Morita, F. J. Giessibl, and R. Wiesendanger, *NCAFM Vol.2, Springer*, edited by S. Morita, F. J. Giessibl, and R. Wiesendanger, NanoScience and Technology (Springer, Berlin, 2009).

[8] J. V. Lauritsen, A. S. Foster, G. H. Olesen, M. C. Christensen, A. Kühnle, S. Helveg, J. R. Rostrup-Nielsen, B. S. Clausen, M. Reichling, and F. Besenbacher, Nanotechnology **17**, 3436 (2006).

[9] C. L. Pang, O. Bikondoa, D. S. Humphrey, A. C. Papageorgiou, G. Cabailh, R. Ithnin, Q. Chen, C. A. Muryn, H. Onishi, and G. Thornton, Nanotechnology **17**, 5397 (2006).

[10] G. H. Enevoldsen, A. S. Foster, M. C. Christensen, J. V. Lauritsen, and F. Besenbacher, Phys. Rev. B **76**, 205415 (2007).

[11] R. Bechstein, C. González, J. Schütte, P. Jelínek, R. Pérez, and A. Kühnle, Nanotechnology **20**, 505703 (2009).

[12] A. Yurtsever, Y. Sugimoto, M. Abe, and S. Morita, Nanotechnology **21**, 165702 (2010).

[13] A. S. Foster, A. Y. Gal, J. M. Airaksinen, O. H. Pakarinen, Y. J. Lee, J. D. Gale, A. L. Shluger, and R. M. Nieminen, Phys. Rev. B **68**, 195420 (2003).

[14] C. Barth, A. S. Foster, C. R. Henry, and A. L. Shluger, Adv. Mater. **23**, 477 (2010).

[15] G. H. Enevoldsen, H. P. Pinto, A. S. Foster, M. C. R. Jensen, A. Kühnle, M. Reichling, W. A. Hofer, J. V. Lauritsen, and F. Besenbacher, Phys. Rev. B **78**, 045416 (2008).

[16] M. A. Lantz, H. J. Hug, R. Hoffmann, P. J. van Schendel, P. Kappenberger, S. Martin, A. Baratoff, and H. J. Güntherodt, Science **291**, 2580 (2001).

[17] B. J. Albers, T. C. Schwendemann, M. Z. Baykara, N. Pilet, M. Liebmann, E. I. Altman, and U. D. Schwarz, Nat. Nanotechnol. **4**, 307 (2009).

[18] R. Hoffmann, M. A. Lantz, H. J. Hug, P. J. A. van Schendel, P. Kappenberger, S. Martin, A. Baratoff, and H.-J. Güntherodt, Phys. Rev. B **67**, 085402 (2003).

[19] R. Hoffmann, L.N. Kantorovich, A. Baratoff, H. J. Hug, and H.-J. Güntherodt, Phys. Rev. Lett. **92**, 146103 (2004).

[20] K. Ruschmeier, A. Schirmeisen, and R. Hoffmann, Phys. Rev. Lett. **101**, 156102 (2008).

[21] R. Hoffmann, D. Weiner, A. Schirmeisen, and A. S. Foster, Phys. Rev. B **80**, 115426 (2009).

[22] G. Teobaldi, K. Lämmle, T. Trevethan, M. Watkins, A. Schwarz, R. Wiesendanger, and A. L. Shluger, Phys. Rev. Lett. **106**, 216102 (2011).

[23] Y. Sugimoto, P. Pou, M. Abe, P. Jelinek, R. Pérez, S. Morita, and O. Custance, Nature (London) **446**, 64 (2007).

[24] M. Ashino, A. Schwarz, T. Behnke, and R. Wiesendanger, Phys. Rev. Lett. **93**, 136101 (2004).

[25] M. Ondráček, P. Pou, V. Rozsíval, C. González, P. Jelínek, and R. Pérez, Phys. Rev. Lett. **106**, 176101 (2011).

[26] N. Suehira, Y. Tomiyoshi, Y. Sugawara, and S. Morita, Rev. Sci. Instrum. **72**, 2971 (2001).

[27] T. R. Albrecht, P. Grütter, D. Horne, and D. Rugar, J. Appl. Phys. **69**, 668 (1991).

[28] M. Abe, Y. Sugimoto, O. Custance, and S. Morita, Nanotechnology **16**, 3029 (2005).

[29] Y. Sugimoto, O. Custance, S. Morita, M. Abe, P. Pou, P. Jelinek, and R. Pérez, Phys. Rev. B **73**, 205329 (2006).

[30] J. E. Sader and S. P. Jarvis, Appl. Phys. Lett. **84**, 1801 (2004).

[31] G. Kresse and J. Furthmüller, Phys. Rev. B **54**, 11169 (1996).

[32] J. P. Perdew, K. Burke, and M. Ernzerhof, Phys. Rev. Lett. **77**, 3865 (1996).

[33] P. Pou, S. A. Ghasemi, P. Jelinek, T. Lenosky, S. Goedecker, and R. Perez, Nanotechnology **20**, 264015 (2009).

[34] M. J. Lundqvist, M. Nilsing, and P. Persson, Int. J. Quantum Chem. **106**, 3214 (2006).

[35] S. Grimme, J. Comp. Chem. **27**, 1787 (2006).

[36] J. C. Conesa, J. Chem. Phys. C **114**, 22718 (2010).